Composites: Part B 43 (2012) 914–925

Contents lists available at SciVerse ScienceDirect

Composites: Part B

journal homepage: www.elsevier.com/locate/compositesb

Prediction of biaxial failure envelopes for composite laminates based on Generalized Method of Cells

Zhanwen Tang [a,*], Boming Zhang [b]

[a] Center for Composite Materials and Structures, Harbin Institute of Technology, Harbin 150001, China
[b] School of Materials Science and Engineering, Beihang University, Beijing 100191, China

ARTICLE INFO

Article history:
Received 24 July 2011
Received in revised form 21 December 2011
Accepted 2 January 2012
Available online 11 January 2012

Keywords:
B. Interface/interphase
B. Strength
B. Microstructures
Micromechanics

ABSTRACT

Macro/micromulti-scale analysis based on the efficient implementation of the Generalized Method of Cells coupled with classical lamination theory was conducted to predict failure of composite laminates, applying failure criteria at the constituent level, including fiber, matrix and interface. Representative unit cells with different fiber arrays were constructed in order to study the effect of reinforcement architecture and failure criteria on strength prediction of composite laminates. In order to compare the micromechanics model's accuracy with commonly-used macroscopic failure theories, the experimental data obtained from the Worldwide Failure Exercise (WWFE) was utilized, and a quantitative assessment method for failure envelopes was developed to evaluate the model's performance. Finally, the types of representative unit cell architectures and failure theories which are applicable for different layups were identified. The results indicate that the predictive performance of the employed micromechanics-based model is closest to the three leading macroscopic failure criteria of Puck, Cuntze and Tsai–Wu, and better than all other microscopic-based failure criteria (Chamis, Mayes, Huang), employed in the WWFE study.

1. Introduction

Fiber-reinforced composite materials have been widely used in the aerospace and aviation industry owing to their superior mechanical properties. The macroscopic mechanical properties and failure mechanisms are closely related to the microstructures [1]. Prediction of failure envelopes of composite laminates is a complex mechanical problem. In order to verify various failure theories, experimental results obtained from the Worldwide Failure Exercise (WWFE) [2–6] were employed in the present study. The WWFE was a comprehensive experimental study that covered a wide range of polymer matrix composite laminates. Specifically, different types of composite materials fabricated using a wide range of fiber and polymeric matrices, laminate lay-ups (unidirectional, angle-ply, cross-ply, quasi-isotropic), and loading conditions were employed. The WWFE data was then compared with the different failure theory predictions from various authors.

It should be noted that the WWFE was mainly geared towards macroscopic (ply level) failure analysis methods with parameters needed to be determined through experimental data. Only three microscopic failure theories (Chamis, Mayes, and Huang) were employed in WWFE, but their performance was not satisfactory. Hence, a need exists for a coupled multi-scale macro/micro-continuum mechanics theory to accurately predict the strength of fiber-reinforced composite materials at the macroscopic and microscopic levels.

In this paper, an efficient predictive model based on the Generalized Method of Cells (GMC) is presented, which allows multi-scale analysis of composites with various fiber arrays. The model contains thousands of subcells, so different constituent materials such as fiber, matrix and interphase can be taken into consideration in each subcell. Four typical representative unit cells with fiber, matrix and interphase failure criterion were developed.

The GMC model with an incorporated interface has been employed to predict failure envelopes of composite laminates when basic fiber, matrix and interphase elastic and strength properties are provided. A quantitative evaluation method is also presented in order to compare the GMC-based model predictions with WWFE failure theories. Finally, the accuracy and suitability of the GMC model are demonstrated through comprehensive comparison with WWFE experimental data.

2. Multi-scale macro/micro-prediction model

The original GMC micromechanics model was developed by Paley and Aboudi [7] for predicting the response of unidirectional metal matrix composites with periodic microstructures. Subsequently, Pindera and Bednarcyk [8] have reformulated the GMC equations using subcell traction components as the unknown

* Corresponding author.
E-mail address: tangzhanwen@163.com (Z. Tang).

1359-8368/$ - see front matter © 2012 Elsevier Ltd. All rights reserved.
doi:10.1016/j.compositesb.2012.01.003

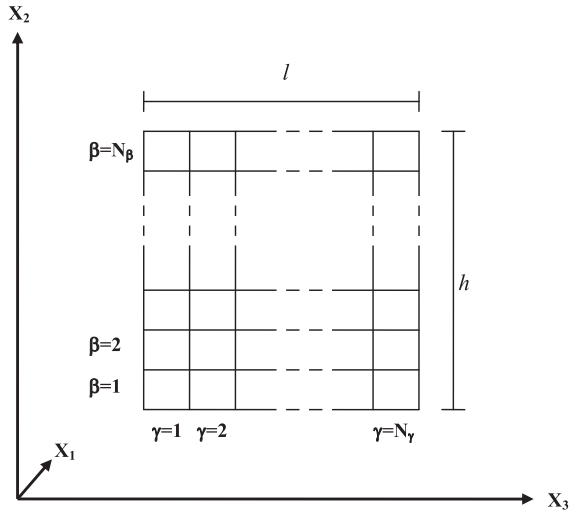

Fig. 1. Discretization of the repeating unit cell.

variables, which produced a computationally optimized GMC with a high level of efficiency and complex unit cell architecture capability. Multi-scale modeling of materials with random microstructure, stochastic simulation of material properties and computational stochastic mechanics based on the moving-window concept were studied by Graham–Brady [9].

2.1. Micromechanics models of GMC

A continuously reinforced composite is modeled as a doubly periodic assemblage of fibers embedded in a matrix phase. The rectangular RUC, depicted in Fig. 1, consists of an arbitrary number of rectangular subcells, denoted by the indices $(\beta\gamma)$, each of which may contain a distinct homogeneous material. The local (subcell) constitutive equation is given by

$$\sigma^{(\beta\gamma)} = C^{(\beta\gamma)}\left(\varepsilon^{(\beta\gamma)} - \varepsilon^{T(\beta\gamma)}\right) \tag{1}$$

where $\sigma^{(\beta\gamma)}$ is the vector of average subcell stresses, $C^{(\beta\gamma)}$ is the subcell elastic stiffness matrix, and $\varepsilon^{(\beta\gamma)}$, $\varepsilon^{T(\beta\gamma)}$ are the vectors of average subcell total and thermal strains, respectively.

A governing system of equations that relates the unknown subcells strains to the macroscopic strains is obtained through the average strain theorem applied to each row and column of the RUC in conjunction with periodicity and traction continuity conditions. This system of equations may be re-cast using normal or shear traction components as the basic unknowns for optimized efficiency as follows:

$$\mathrm{GT} = f^m - f^T \tag{2}$$

where the G matrix contains information on the subcell material elastic properties and the subcell dimensions, the T vector are the unique subcell stress components, the f^m vector contains information on the repeating unit cell dimensions and the global (unit cell) strains, f^T vector contains the thermal effects.

Once Eq. (2) are solved, the local stress and strain fields throughout the repeating unit cell can be determined from the local constitutive Eq. (1). Then the terms in the global constitutive equation:

$$\bar{\sigma} = C^*(\bar{\varepsilon} - \bar{\varepsilon}^T) \tag{3}$$

can be determined using the definition of average (global) stress,

$$\bar{\sigma} = \frac{1}{hl}\sum_{\beta=1}^{N_\beta}\sum_{\gamma=1}^{N_\gamma} h_\beta l_\gamma \bar{\sigma}^{(\beta\gamma)} \tag{4}$$

where C^* is the effective stiffness matrix, $\bar{\varepsilon}, \bar{\varepsilon}^T$ are the effective total, thermal strain vectors.

2.2. Multi-scale macro/microanalysis model based on GMC

Four typical RUCs were employed in this paper, as shown in Fig. 2. The RUCs coupled with classical lamination theory were used to predict failure strength of composite laminates. The sequence of calculations is listed below:

(1) Compute the effective stiffness matrix of the fibrous composite from the fiber, matrix and interphase material properties (degraded stiffness matrix is adopted if material has been damaged).
(2) Calculate macro-stress/strain of ply-level using classical lamination theory.

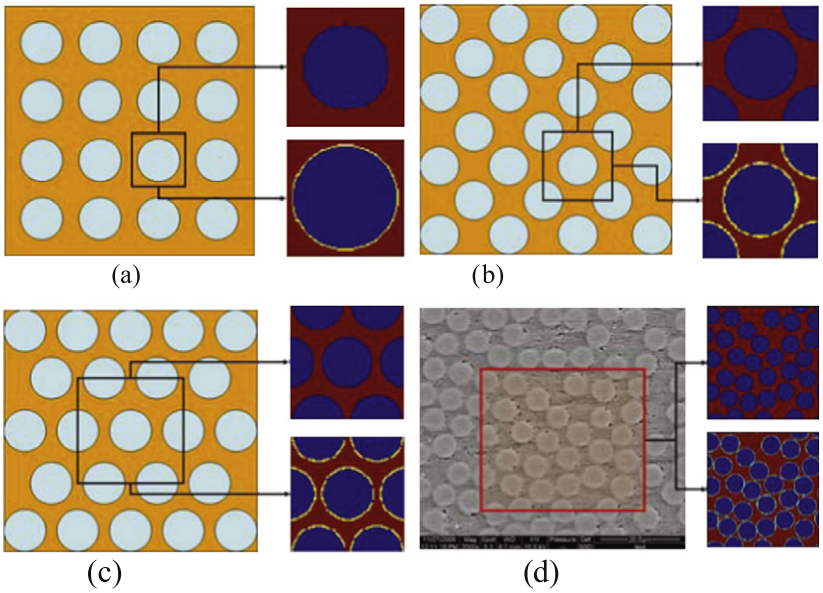

Fig. 2. Repeating unit cells with different arrays of circular fibers (a) square arrays, (b) square-diagonal arrays, (c) hexagonal arrays, (d) random arrays.

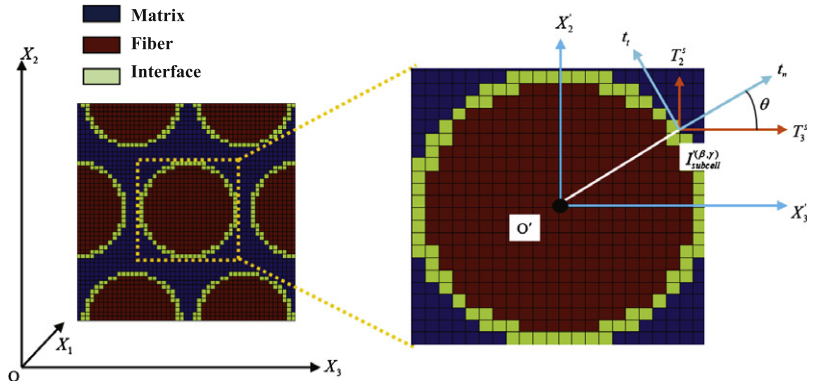

Fig. 3. Illustration of stresses components in normal and tangential directions of interface.

(3) Apply boundary conditions in the form of macroscopic strain obtained from previous step to the RUC representing each ply in the laminate to calculate subcell stresses.
(4) Apply micro-level failure criteria to determine whether RUC material points represented by subcells are damaged or failure occurs. The subcell material points are utilized to track and integrate the nonlinear effects associated with damage, debonding, and inelasticity, which vary arbitrarily within a ply in the general loading case involving damage.
(5) Calculate the effective stiffness matrix, and then determine whether final failure occurs, if final failure has occurred, then go to the final step, else go back to step 1 (with the degraded stiffness) to continue the loop.
(6) Final failure load is determined.

Laminate constitutive equations can be expressed as follows:

$$\begin{bmatrix} A & B \\ B & D \end{bmatrix} \begin{bmatrix} \varepsilon \\ k \end{bmatrix} = \begin{bmatrix} N \\ M \end{bmatrix} \tag{5}$$

where A, B and D are the effective extension, coupling, and bending stiffness matrices of the laminate, ε, k are vectors containing the mid-plane strain and curvature components, N, M are the force and moment vectors.

2.3. The interfacial damage/debonding model

2.3.1. Fiber–matrix interface failure criterion

The following condition is employed to determine whether the fiber–matrix interface has been damaged

$$\left(\frac{\langle t_n \rangle}{Y_n}\right)^2 + \left(\frac{t_t}{Y_t}\right)^2 + \left(\frac{t_l}{Y_l}\right)^2 = 1 \tag{6}$$

where angular brackets $\langle\rangle$ stand for the Macaulay brackets, which return the argument if positive and zero otherwise, so that there will be no damage at the interface when the interface is under compression. t_n, t_t, t_l indicate interfacial tractions in normal, tangential (to the circumference), and longitudinal directions, respectively, while Y_n, Y_t, Y_l represent the maximum allowable values of interfacial tractions in those three directions, respectively [10].

2.3.2. Stress components of interface

The stresses utilized in the fiber/matrix failure criterion are obtained from the lamination theory analysis in the global coordinate system, but the stresses applied in the interface failure criterion are expressed in the local coordinate system with the origin at the center of the fiber, as shown in Fig. 3. In the figure, o' represents the origin of the local coordinates and $I_{subcell}^{\prime(\beta,\gamma)}$ represents an interface subcell containing interfacial material

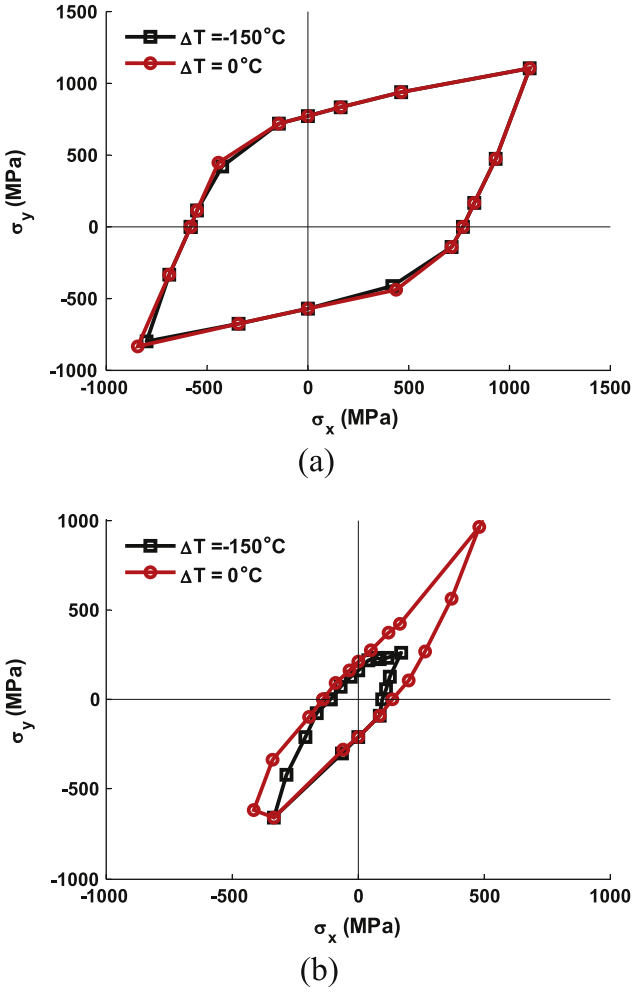

Fig. 4. Failure envelopes based on GMC for laminate taking into account the thermal residual stresses (a) Failure envelopes for $[90°/\pm45°/0°]_s$ laminate and (b) failure envelopes for $[55°/-55°]_s$ laminate.

properties. The direction of the line connecting o' and $I_{subcell}^{\prime(\beta,\gamma)}$ is normal to the interface, and the normal interfacial tractions t_n are comprised of the global stress vector components (T_2^s, T_3^s) resolved along the normal directions, see by Eq. (7). The tangential interfacial tractions t_t are comprised of the global stresses vector components (T_2^s, T_3^s) resolved along the tangential directions, see Eq. (8). The interfacial traction t_l in the longitudinal direction is the same as the global stress vector T_1^s. In the equations below, θ is the angle between lines $o'I_{subcell}^{\prime(\beta,\gamma)}$ and local axis T_2^s.

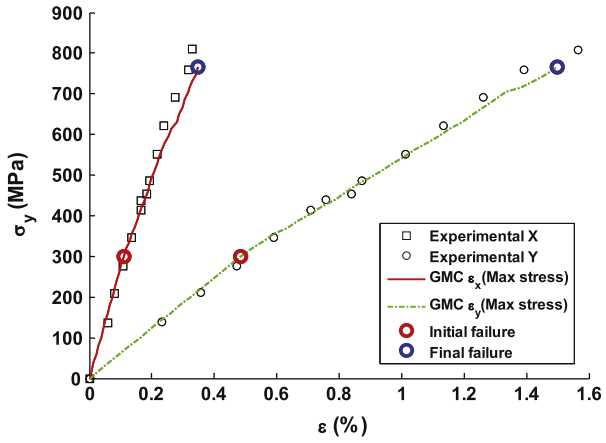

Fig. 5. $[90°/\pm45°/0°]_s$ laminate AS4/3501-6: stress/strain curves for $\sigma_y/\sigma_x = 2/1$ with GMC.

$$t_n = T_2^s \sin(\theta) + T_3^s \cos(\theta) \tag{7}$$

$$t_t = T_2^s \cos(\theta) + T_3^s \sin(\theta) \tag{8}$$

$$t_l = T_1^s \tag{9}$$

Applying the above equations, all interfacial traction components in the representative unit cell can be determined. Then the interfacial tractions t_n, t_t and t_l, which are obtained from Eqs. (7)–(9), are substituted into the failure criterion Eq. (6) to determine whether the failure criterion is satisfied. If the condition is satisfied, the interface is then considered damaged/debonded. Y_n, Y_t and Y_l need to be provided by the user.

2.4. Failure theories used at the fiber/matrix level

The employed failure theories are outlined herein, all of which are applied at the fiber/matrix constituent level. In the sequel, $X_{C\varepsilon}$, $X_{T\varepsilon}$ and $X_{S\varepsilon}$ are the compressive, tensile and shear strain limits, respectively. Similarly, X_C, X_T and X_S are the compressive, tensile and shear strengths.

Table 2
Material mechanical properties of fiber.

Fiber	AS4	T300	E-glass Gevetex	Silenka E-glass
Axial modulus E_{f1} (GPa)	225	230	80	74
Transverse modulus E_{f2} (GPa)	15	15	80	74
Shear modulus in-plane G_{f12} (GPa)	15	15	33.33	30.8
Transverse shear modulus G_{f23} (GPa)	7	7	33.33	30.8
Poisson's ratio	0.2	0.2	0.2	0.2
Axial tensile strength X_{fT} (MPa)	3350	25,000	2150	2150
Axial compressive strength X_{fC} (MPa)	2500	2000	1450	1450
Axial tensile strain limit ε_{f1T} (%)	1.488	1.086	2.687	2.905
Axial compressive strain limit ε_{f1C} (%)	1.111	0.869	1.813	1.959

2.4.1. Matrix constituent failure theories

(1) Maximum strain criteria

$$\begin{aligned} &X_{C\varepsilon} < \varepsilon_{11} < X_{T\varepsilon} \quad |\gamma_{23}| < X_{S\varepsilon} \\ &X_{C\varepsilon} < \varepsilon_{22} < X_{T\varepsilon}, \quad |\gamma_{13}| < X_{S\varepsilon} \\ &X_{C\varepsilon} < \varepsilon_{33} < X_{T\varepsilon} \quad |\gamma_{12}| < X_{S\varepsilon} \end{aligned} \tag{10}$$

(2) Maximum stress criteria

$$\begin{aligned} &X_C < \sigma_{11} < X_T \quad |\tau_{23}| < X_S \\ &X_C < \sigma_{22} < X_T \quad |\tau_{13}| < X_S \\ &X_C < \sigma_{33} < X_T \quad |\tau_{12}| < X_S \end{aligned} \tag{11}$$

(3) Tsai–Hill criteria [11]

$$\begin{aligned} &\frac{\sigma_{11}^2}{X^2} + \frac{\sigma_{22}^2}{Y^2} + \frac{\sigma_{33}^2}{Z^2} + \frac{\tau_{23}^2}{X_S^2} + \frac{\tau_{12}^2}{X_S^2} + \frac{\tau_{13}^2}{X_S^2} \\ &- \sigma_{11}\sigma_{22}\left(\frac{1}{X^2} + \frac{1}{Y^2} - \frac{1}{Z^2}\right) - \sigma_{11}\sigma_{33}\left(\frac{1}{X^2} - \frac{1}{Y^2} + \frac{1}{Z^2}\right) \\ &- \sigma_{22}\sigma_{33}\left(-\frac{1}{X^2} + \frac{1}{Y^2} + \frac{1}{Z^2}\right) \end{aligned} \tag{12}$$

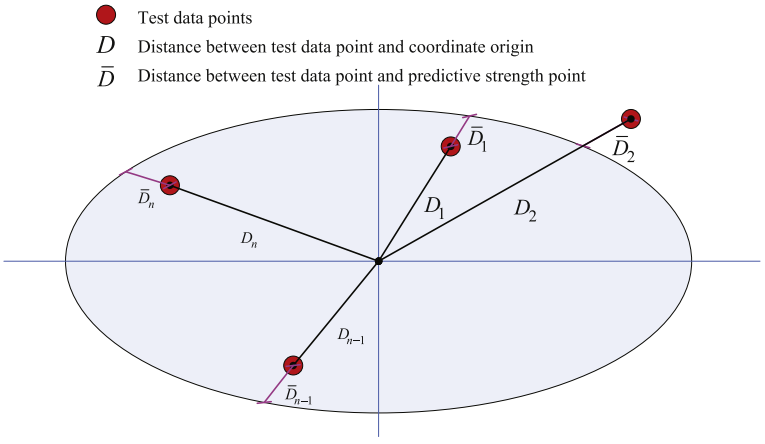

Fig. 6. Schematic diagram of the assessment method of failure envelopes.

Table 1
Assessment method of biaxial failure envelops.

Error	$0 < k_i \leqslant 0.1$	$0.1 < k_i \leqslant 0.2$	$0.2 < k_i \leqslant 0.3$	$0.3 < k_i \leqslant 0.4$	$0.4 < k_i \leqslant 0.5$	$0.5 < k_i \leqslant 0.6$	$0.6 < k_i \leqslant 0.7$	$0.7 < k_i \leqslant 0.8$	$0.8 < k_i \leqslant 0.9$	$0.9 < k_i \leqslant 1.0$	$k_i > 1.0$
Grade	10	9	8	7	6	5	4	3	2	1	0

Table 3
Material mechanical properties of matrix.

Matrix	3501-6 epoxy	BSL914 epoxy	LY556/HT907/DY063 epoxy	MY750/HY917/DY063 epoxy
Axial modulus E_m (GPa)	4.2	4.0	3.35	3.35
Shear modulus in-plane G_m (GPa)	1.567	1.481	1.24	1.24
Poisson's ratio v_m	0.34	0.35	0.35	0.35
Axial tensile strength Y_{mT} (MPa)	69	75	80	80
Axial compressive strength Y_{mC} (MPa)	250	150	120	120
Shear strength S_m (MPa)	50	70	–	–
Axial tensile strain limit ε_{mT} (%)	1.7	4	5	5

Table 4
Summary of laminate types, material types.

Laminate (lay-up)	Lamina	Material
$[0°]_n$	>0	Silenka/MY750 epoxy
$[90°/30°/-30°]_s$	90° lamina:0.172 mm 30° lamina:0.414 mm	Gevetex Eiglass/LY556 epoxy
$[90°/\pm45°/0°]_s$	Lamina:0.1375 mm	AS4/3501-6 epoxy
$[55°/-55°]_s$	Lamina:0.25 mm	Silenka/MY750 epoxy
$[0°/90°/0°]_s$	0° lamina:0.25 mm 0° lamina:0.5 mm	Silenka/MY750 epoxy

In the above,

$$X=\begin{cases}X_T;\ \sigma_{11}\geqslant 0\\ X_C;\ \sigma_{11}<0\end{cases},\quad Y=\begin{cases}X_T;\ \sigma_{22}\geqslant 0\\ X_C;\ \sigma_{22}<0\end{cases},\quad Z=\begin{cases}X_T;\ \sigma_{33}\geqslant 0\\ X_C;\ \sigma_{33}<0\end{cases}$$

(4) Tsai–Wu criteria [12]

$$\sigma_{11}\left(\frac{1}{X_T}+\frac{1}{X_C}\right)+\sigma_{22}\left(\frac{1}{X_T}+\frac{1}{X_C}\right)+\sigma_{33}\left(\frac{1}{X_T}+\frac{1}{X_C}\right)-\frac{\sigma_{11}^2}{X_TX_C}-\frac{\sigma_{22}^2}{X_TX_C}-\frac{\sigma_{33}^2}{X_TX_C}+\frac{\tau_{23}^2}{X_S^2}+\frac{\tau_{13}^2}{X_S^2}+\frac{\tau_{12}^2}{X_S^2}+\frac{\sigma_{11}\sigma_{22}}{X_TX_C}+\frac{\sigma_{11}\sigma_{33}}{X_TX_C}+\frac{\sigma_{22}\sigma_{33}}{X_TX_C}=1 \tag{13}$$

(5) Hashin–Rotem 2D criteria [13]

$$\left(\frac{\sigma_{22}}{X_T}\right)^2+\left(\frac{\tau_{12}}{X_S}\right)^2=1,\ \sigma_{22}>0;\quad \left(\frac{\sigma_{22}}{X_C}\right)^2+\left(\frac{\tau_{12}}{X_S}\right)^2=1,\ \sigma_{22}<0 \tag{14}$$

(6) Hashin–Rotem 3D criteria [13]

$$\left(\frac{\sigma_{22}}{X_T}\right)^2+\left(\frac{\sigma_{33}}{X_T}\right)^2+\left(\frac{\tau_{12}}{X_S}\right)^2+\left(\frac{\tau_{13}}{X_S}\right)^2+\left(\frac{\tau_{23}}{X_S}\right)^2=1,\quad \sigma_{22}+\sigma_{33}>0$$
$$\left(\frac{\sigma_{22}}{X_C}\right)^2+\left(\frac{\sigma_{33}}{X_C}\right)^2+\left(\frac{\tau_{12}}{X_S}\right)^2+\left(\frac{\tau_{13}}{X_S}\right)^2+\left(\frac{\tau_{23}}{X_S}\right)^2=1,\quad \sigma_{22}+\sigma_{33}>0 \tag{15}$$

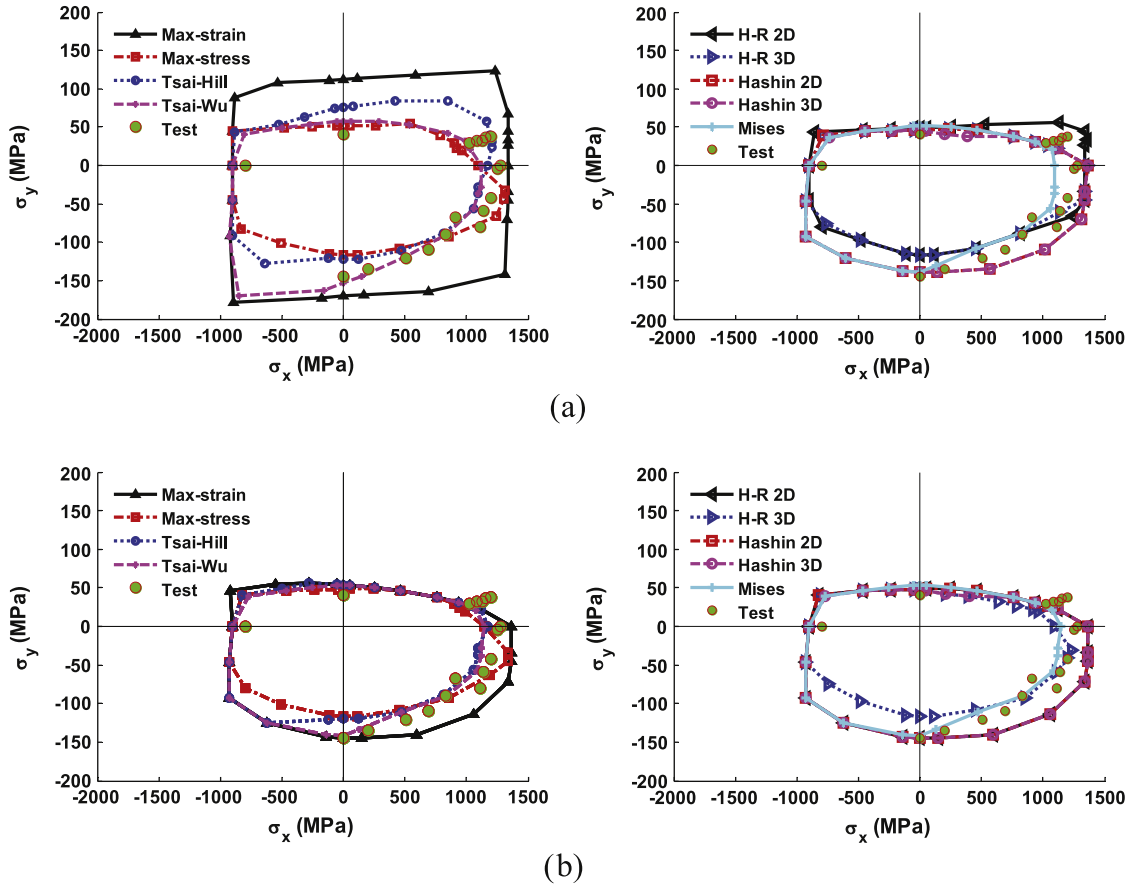

Fig. 7. Failure envelopes based on GMC for $[0°]_n$ lamina (a) repeating unit cell with square arrays (without interface) and (b) repeating unit cell with square arrays (with interface).

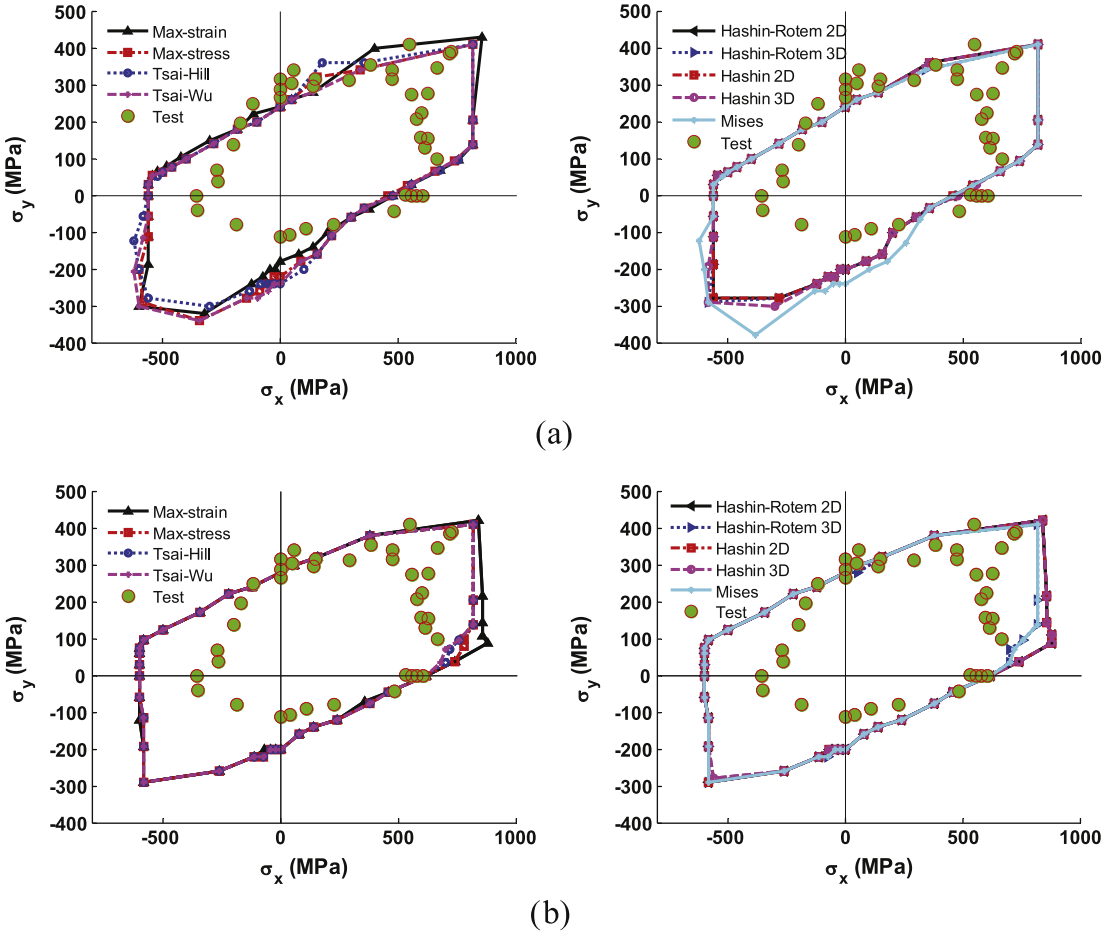

Fig. 8. Failure envelopes based on GMC for $[90°/30°/-30°]_s$ laminate (a) repeating unit cell with square arrays (without interface) and (b) repeating unit cell with square arrays (with interface).

(7) Hashin 2D criteria [14]

$$\left(\frac{\sigma_{22}}{X_T}\right)^2+\left(\frac{\tau_{12}}{X_S}\right)^2=1,\ \sigma_{22}\geqslant 0$$
$$\left(\frac{\sigma_{22}}{2X_S}\right)^2+\left[\left(\frac{Y^C}{2X_S}\right)^2-1\right]\frac{\sigma_{22}}{X_C}+\left(\frac{\tau_{12}}{X_S}\right)^2=1,\ \sigma_{22}\leqslant 0 \tag{16}$$

(8) Hashin 3D criteria [14]

$$\frac{1}{X_T^2}(\sigma_2+\sigma_3)^2+\frac{1}{X_S^2}(\tau_{23}^2-\sigma_2\sigma_3)+\frac{1}{X_S^2}(\tau_{12}^2+\tau_{13}^2)=1,\ (\sigma_2+\sigma_3)>0$$
$$\frac{1}{X_C}\left[\left(\frac{X_C}{2X_S}\right)^2-1\right](\sigma_2+\sigma_3)+\frac{1}{4X_S^2}(\sigma_2+\sigma_3)^2$$
$$+\frac{1}{X_S^2}(\tau_{23}^2-\sigma_2\sigma_3)+\frac{1}{X_S^2}(\tau_{12}^2+\tau_{13}^2)=1,\ (\sigma_2+\sigma_3)<0 \tag{17}$$

(9) Mises criteria [15]

$$\left(\frac{\sigma_{VM}}{\sigma_{VM}^{cr}}\right)^2+\left(\frac{I_1}{I_1^{cr}}\right)^2=1 \tag{18}$$

where

$$I_1=\sigma_1+\sigma_2+\sigma_3, I_2=\sigma_1\sigma_2+\sigma_2\sigma_3+\sigma_3\sigma_1-(\tau_{23}^2+\tau_{12}^2+\tau_{13}^2)$$

$$\sigma_{VM}=\sqrt{I_1^2-3I_2},\ \sigma_{VM}^{cr}=\sqrt{X_TX_C},\ I_1^{cr}=\frac{X_TX_C}{X_C-X_T}$$

2.4.2. Fiber constituent failure theory

Due to the unidirectional fiber reinforcement at the ply level, just one failure criteria for the fiber phase is employed, namely

$$\left(\frac{\sigma_{11}}{X_T}\right)^2=1\sigma_{11}\geqslant 0;\ \left(\frac{\sigma_{11}}{X_C}\right)^2=1\sigma_{11}<0 \tag{19}$$

2.5. Influence of thermal residual stresses on failure envelopes

It is well known that thermal residual stresses always exist in composites because of the mismatch in the thermal expansion coefficients between different components or different layers. In multidirectional laminates, for example, residual stresses may contribute to the initial and final failure. Hence biaxial failure envelopes for $[0°]_n$ lamina, $[90°/30°/-30°]_s$ laminate, $[90°/\pm45°/0°]_s$ laminate and $[55°/-55°]_s$ were generated to determine the influence of thermal residual stresses on failure envelopes. The main conclusions of this study are summarized below:

(1) Thermal residual stresses have substantial influence on the initial failure of the four laminates.
(2) Thermal residual stresses have little influence on final failure envelopes of $[90°/30°/-30°]_s$ and $[90°/\pm45°/0°]_s$ laminates, while greater effect is observed in the case of $[0°]_n$ and $[55°/-55°]_s$ laminates.

Fig. 4 compares the effect of thermal residual stresses on the failure envelope of $[90°/\pm45°/0°]_s$ and $[55°/-55°]_s$ laminates to illustrate the extent of the difference.

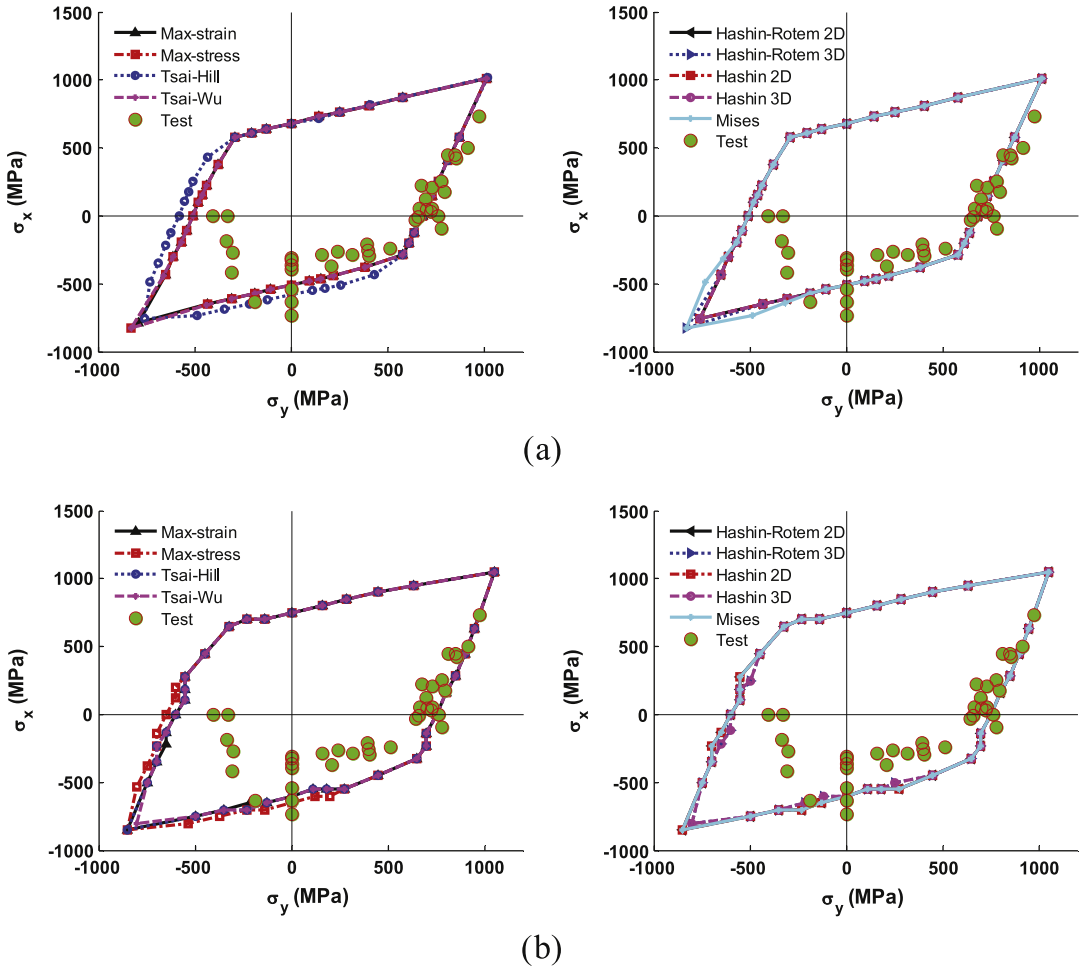

Fig. 9. Failure envelopes based on GMC for $[90°/\pm45°/0°]_s$ laminate (a) repeating unit cell with square arrays (without interface) and (b) repeating unit cell with square arrays (with interface).

2.6. Prediction and quantitative assessment method of failure envelopes

In order to illustrate how the failure envelopes based on progressive failure have been calculated, a typical macroscopic stress–strain curve of a $[90°/\pm45°/0°]_s$ laminate has been generated for the radial loading path $\sigma_y/\sigma_x = 2/1$, see Fig. 5. In this paper, the failure envelopes were based on final failure as shown in the figure. A quantitative assessment method of failure envelopes based on experimental data was developed to evaluate the performance of the GMC-based model, and the basic idea is shown in Fig. 6. Red dots represent experimental data points, D_i represents distance between the coordinates of the origin and the test data; $\overline{D}_i$ represents the distance between test data point and predicted strength point. The error is defined as $k_i = |\overline{D}_i|/D_i$ based on which the grades are assigned corresponding to different errors. The thus defined assessment criteria of failure envelopes are summarized in Table 1.

3. GMC-based prediction of failure envelopes

The material properties of the constituents used in this paper were taken from the WWFE study [2–5]. They are given in Tables 2 and 3. The laminate types and material types are listed in Table 4.

The GMC-based unit cell models coupled with the classical lamination theory are employed to predict the WWFE laminate behavior. The strength criteria employed for the constituent materials include one fiber strength criterion, one fiber/matrix interface strength criterion and nine matrix strength criteria. The focus of the study is the influence of the nine matrix failure theories and the interface strength on the laminate failure envelopes, as well as the quantitative assessment of the predicted failure envelopes by the implemented micromechanics-based approach. It is stressed that no modifications have been made to account for the in situ behavior of the constituents, pure predictions have been made using the constituent properties provided by the WWFE, and thermal residual stresses due to the temperature change $\Delta T = -150\,°C$ have been included. Furthermore, the simplest damage progression model has been employed at the microscale. That is, once a subcell within the GMC-based unit cell model satisfies the applicable failure criterion, that subcell is instantaneously assigned a near zero stiffness [16]. In the case of the $[0°]_n$, $[90°/+30°/-30°]_s$ and $[90°/\pm45°/0°]_s$ laminates, the influence of the unit cell fiber architecture is small, and thus the results for these three laminate lay-ups given in Figs. 7–9 are only shown for the square fiber array. In contrast, the failure envelopes of the $[55°/-55°]_s$ laminate are affected by the fiber array type, and hence failure envelopes of all four unit cell architectures are given in Figs. 10 and 11 for this laminate.

Finally, the simulation results have been compared together in order to evaluate the capabilities of the GMC-based multi-scale laminate model. The compared results are listed in Table 5. The left column number represents the matrix failure criteria given in

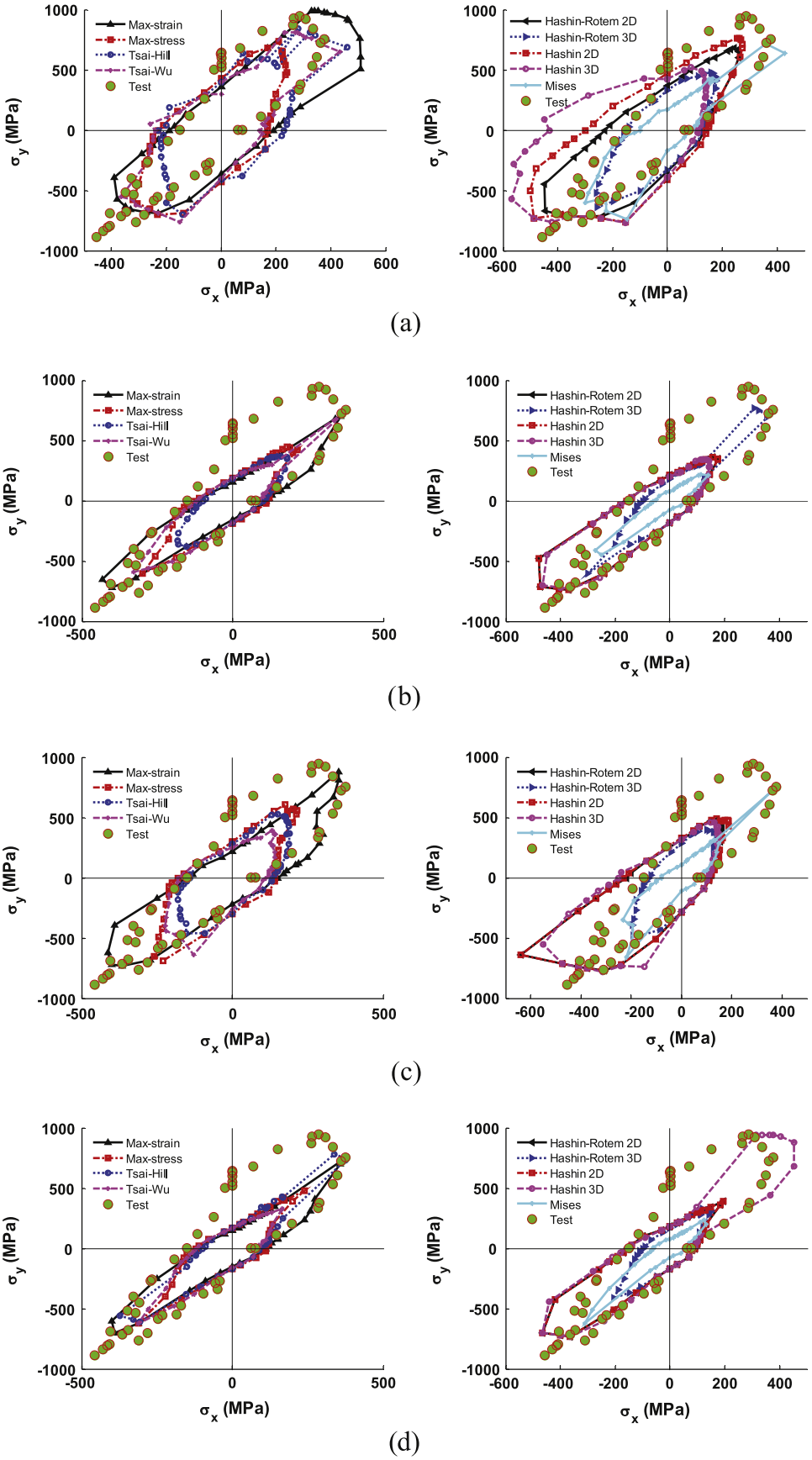

Fig. 10. Failure envelopes based on GMC for $[55°/-55°]_s$ laminate (without interface) (a) repeating unit cell with square arrays, (b) repeating unit cell with square-diagonal arrays, (c) repeating unit cell with hexagonal arrays, (d) repeating unit cell with random arrays.

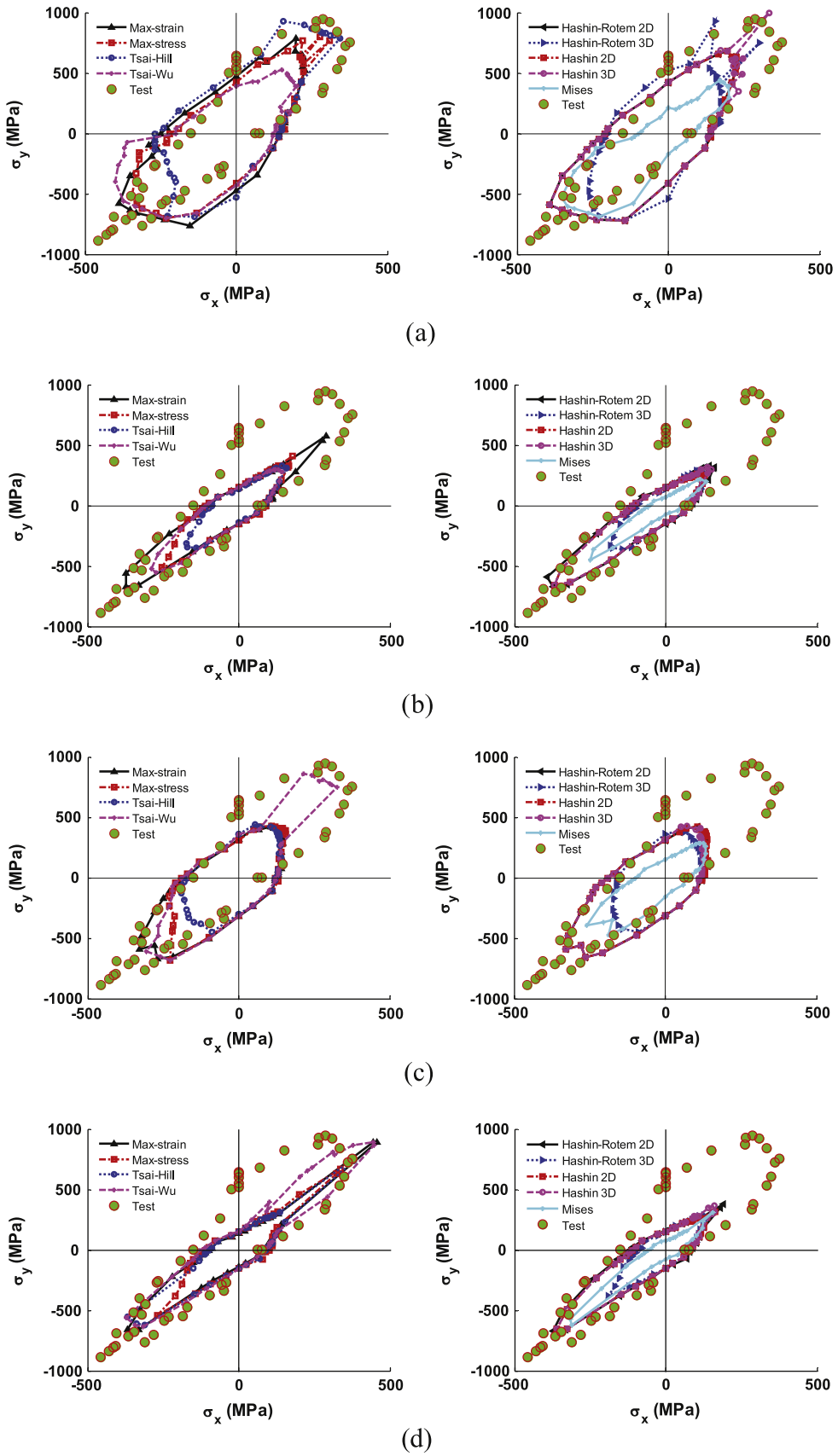

Fig. 11. Failure envelopes based on GMC for $[55°/-55°]_s$ laminate (with interface) (a) repeating unit cell with square arrays, (b) repeating unit cell with square-diagonal arrays, (c) repeating unit cell with hexagonal arrays, (d) repeating unit cell with random arrays.

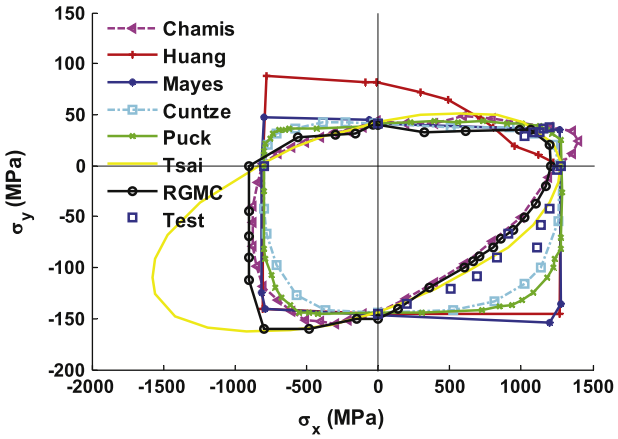

Fig. 12. Failure envelopes for $[0°]_n$ lamina.

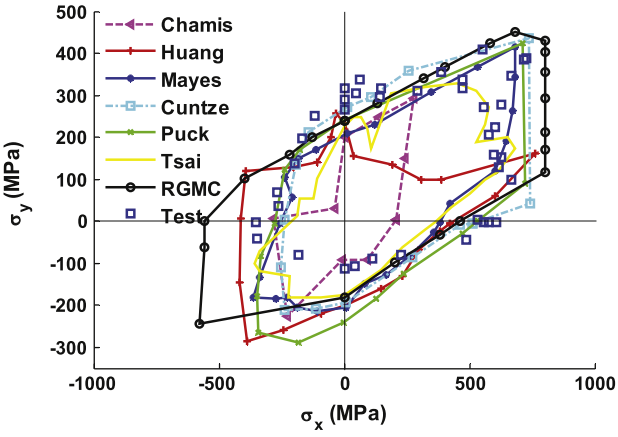

Fig. 13. Failure envelopes for $[90°/30°/-30°]_s$ laminate.

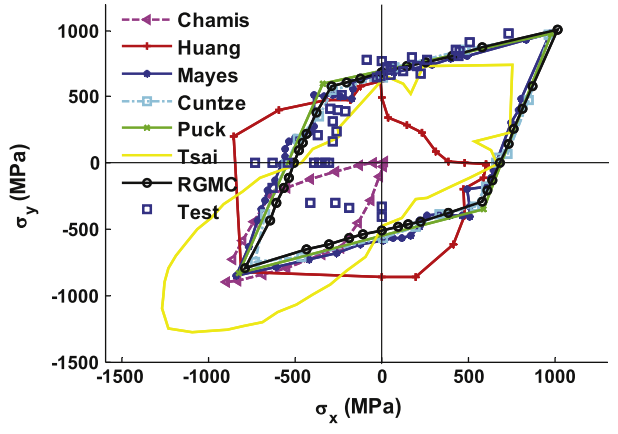

Fig. 14. Failure envelopes for $[90°/\pm45°/0°]_s$ laminate.

Section 2.4. The letters A–D represent the four types of GMC-based unit cell architectures shown in Fig. 2, respectively. The assessment criterion for each laminate type is listed in the first row of Table 1, and the check mark $\surd$ indicates that the criterion is satisfied. The row/column totals represent cumulative quantities, which satisfy the assessment criterion.

Based on the results reported in Table 5, the rankings of the matrix failure criteria from best to worst are as follows: Tsai–Hill,

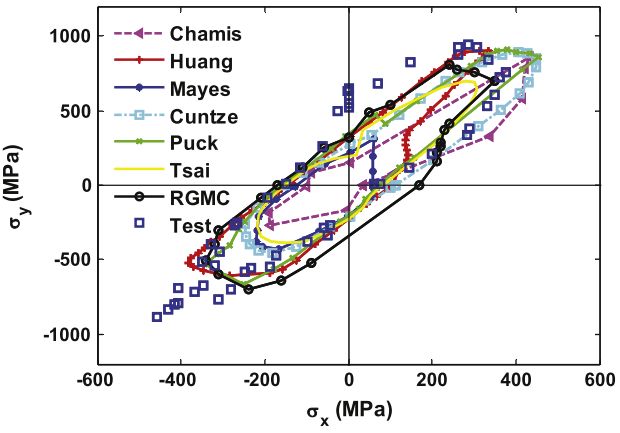

Fig. 15. Failure envelopes for $[55°/-55°]_s$ laminate.

Max-Strain, Hashin 2D, Hashin–Rotem 2D and Hashin 3D, Tsai–Wu, Mises, Hashin–Rotem 3D, Max-Stress.

Furthermore, the square array RUC performs better in predicting failure of unidirectional lamina, and the square and random array RUCs perform better in predicting failure of the $[90°/+30°/-30°]_s$ and $[90°/\pm45°/0°]_s$ laminates. Moreover, the square RUC performs better in predicting failure of the $[55°/-55°]_s$ laminate. On the other hand, square-diagonal and hexagonal array RUCs exhibit medium performance. The performance of the random array model in predicting failure of the $[55°/-55°]_s$ laminate is not satisfactory. The main reason may be that the stiffness degradation method does not adequately describe the progressive failure mechanism. Therefore, the degradation model for a damaged subcell needs further study in our future work.

4. A comparison with failure theories in WWFE

In order to examine the performance of the GMC-based model at the laminate level, three macroscopic failure criteria (Puck, Cuntze and Tsai–Wu) and three microscopic-based failure criteria (Chamis, Mayes, Huang) employed in the WWFE study were chosen for comparison with the present model and comparison results are given in Fig. 12–15. This choice was motivated by the fact that under biaxial loading the above three macroscopic failure criteria yield best predictions relative to experimental data, while there are only three microscopic-based failure criteria used in the WWFE Study.

A comprehensive comparison is made among the failure theories and the results of performance assessment are summarized in Table 6. The results show that the macroscopic failure theories of Puck, Cuntze, and Tsai–Wu perform better than the microscopic-based criteria of Chamis, Mayes, and Huang. However, they require more extensive generation of experimental data for input, and moreover they cannot track the damage evolution at the constituent level such as matrix damage, fiber fracture, and matrix–fiber interface debonding.

On the other hand, the micromechanics failure theories employed in the WWFE study do not perform well and lack universal applicability. For instance, the micromechanics model of Chamis received a score of 9.5 in the case of lamina, but less than 6.0 in other cases. Similarly, the micromechanics model of Mayes received a score of 9.0 in the case of lamina, but 5.28 in the case of $[55°/-55°]_s$ laminate. The performance of Huang's model is the worst among all seven failure criteria adopted except for the score of 7.6 in the case of $[55°/-55°]_s$ laminate.

The presented GMC-based micromechanics model has the capabilities, given the arrangement and properties of the constituent

Table 5
Performance assessment of the GMC-based multi-scale model.

Matrix Criteria	Lamina $[0°]_n$ (grade greater than 8.68)				Laminate $[90°/+30°/-30°]_s$ (grade greater than 7.19)				Laminate $[90°/\pm45°/0°]_s$ (grade greater than 7.65)				Laminate $[55°/-55°]_s$ (grade greater than 6.29)				Total
	A	B	C	D	A	B	C	D	A	B	C	D	A	B	C	D	
1	√	√	√	√	√	√	√	√					√	√	√	√	12
2					√			√					√	√	√		5
3	√		√	√	√	√	√	√	√	√	√	√	√	√	√		14
4	√		√		√	√		√					√	√	√		8
5	√			√	√			√	√	√	√	√	√		√		10
6					√	√	√	√				√	√				6
7	√			√	√			√	√	√	√	√	√	√	√		11
8	√	√		√	√			√	√	√	√	√		√			10
9	√		√		√	√	√	√					√				7
Total	7	2	4	5	9	5	4	9	4	4	4	5	8	6	6	1	

Grade based on the results of Table 1 assessment criteria; 8.68, 7.19, 7.65, and 6.29 is the average score of each lay-up type individually.

Table 6
Results of performance assessment of failure theories.

	Chamis	Huang	Mayes	Cuntze	Puck	Tsai	GMC
Lamina [0°]	9.50	8.28	9.00	9.61	9.33	9.94	9.33
Laminate $[90°/30°/-30°]_s$	5.65	6.13	8.17	8.61	8.43	8.09	7.57
Laminate $[90°/45°/0°]_s$	–	4.62	7.76	8.05	7.76	7.43	7.76
Laminate $[55°/-55°]_s$	5.96	7.60	5.28	7.96	8.44	7.88	7.72
Average	7.04	6.66	7.55	8.56	8.49	8.33	8.10

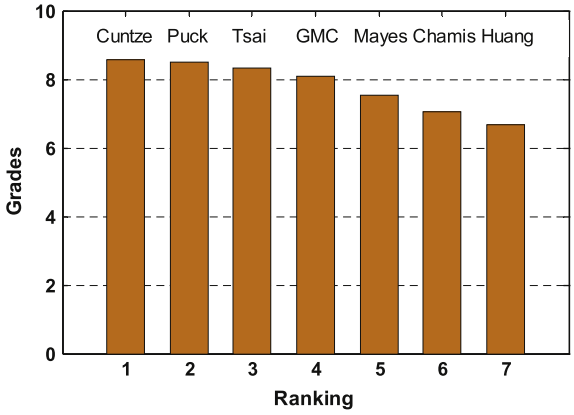

Fig. 16. Performance assessment of failure theories.

materials, to predict failure envelopes of composite laminates with greater accuracy than the above micromechanics models based on various failure mechanisms considered in this study. Moreover, its performance is very close to the three leading macroscopic failure theories employed in the WWFE study (averages are all greater than 8.0). Their averages have been plotted in bar figure in Fig. 16.

5. Conclusions

The objectives of this study were to evaluate the current predictive capabilities of the GMC-based micro–macromechanics model relative to progressive failure evolution in polymer matrix composite laminates. The influence of nine failure criteria applied at the matrix constituent scale and four unit cells with different fiber arrays and fiber/matrix interface debonding capability was also evaluated. In order to evaluate the capabilities of the employed GMC-based multi-scale model, a quantitative evaluation method of failure envelopes was presented. Comparison of the model's predictions based on the incorporated failure theories at the constituent level with the failure criteria employed in the WWFE study was then conducted.

The results indicate that the GMC-based multi-scale model performs well in predicting failure envelopes of composite laminates, with the accuracy of predictions closest to the three leading macro-failure criteria of Puck, Cuntze and Tsai–Wu employed in the WWFE study. It also performs better than the three micromechanics based failure criteria (Chamis, Mayes, Huang) of the above study. The results of this study suggest that the choice of the matrix failure criterion and fiber array architecture has impact on the accuracy of predictions. In particular,

(1) For failure envelopes of $[0°]_n$ laminates, predictions based on Max-strain, Tsai–Hill, Tsai–Wu, Hashin3D, matrix failure criteria and square, random array RUCs produce best results.
(2) For failure envelopes of $[90°/30°/-30°]_s$, $[90°/\pm45°/0°]_s$ laminates, all matrix failure criteria produce similar results, and the predictive results are consistent well with experimental data except these results in the third quadrant ($\sigma_x < 0$ and $\sigma_y < 0$).
(3) For failure envelopes of $[55°/-55°]_s$ laminates, predictions based on Max-strain, Max-stress, Tsai–Hill, Tsai–Wu, Hashin 2D matrix failure criteria and square array RUCs produce best results.

It should also be noted that there are some intrinsic limitations of the GMC model. GMC is essentially a spring model which lacks so-called shear coupling mechanism. Specifically, transverse normal and axial shear stress components are constant along each row and column in the direction travelled; and transverse shear stress is constant throughout the entire unit cell. Therefore, this feature leads to potentially very inaccurate results in the presence of cracks, disbonds or porosities because it eliminates the load-bearing capability of all subcells located in the rows and columns that contain these geometric features. For instance, in the presence of fiber/matrix debonding, the transverse shear modulus for the entire RUC becomes zero. Hence, for those laminates wherein the ply-level shear stress is significant in the material principal coordinate system, GMC will produce very conservative predictions. In such circumstances, a high-fidelity model should be employed to predict failure envelopes of composites, and finite-volume direct averaging micromechanics (FVDAM) theory developed by Bansal and Pindera [17] is a promising choice. Work is currently underway to address these needs.

Acknowledgments

The authors gratefully acknowledge the support provided by Major State Basic Research Development Program of China (973 Program) through the grants No. 2010CB631100. In particular, the authors are indebted to Wenqiong Tu who is a PhD student in the Civil Engineering Department at the University of Virginia for providing assistance with English editing.

References

[1] Boming Z, Zhong Y, Xinyang S, Zhanwen T. A virtual experimental approach to estimate composite mechanical properties: modeling with an explicit finite element method. Comput Mater Sci 2010;49:645–51.
[2] Hinton MJ, Soden PD. Predicting failure in composite laminates: background to the exercise. Compos Sci Technol 1998;58(7):1001–10.
[3] Soden PD, Hinton MJ, Kaddour AS. Lamina properties, lay-up configuration and loading conditions for a range of fibre reinforced composite laminates. Compos Sci Technol 1998;58(7):1011–22.
[4] Soden PD, Hinton MJ, Kaddour AS. A comparison of the predictive capabilities of current failure theories for composite laminates. Compos Sci Technol 1998;58:1225–54.
[5] Soden PD, Hinton MJ, Kaddour AS. Biaxial test results for strength and deformation of a range of E-glass and carbon fibre reinforced composite laminates: failure exercise benchmark data. Compos Sci Technol 2002;62:1489–514.
[6] Kaddoura AS, Hintonb MJ, Soden PD. A comparison of the predictive capabilities of current failure theories for composite laminates: additional contributions. Compos Sci Technol 2004;64:449–76.
[7] Paley M, Aboudi J. Micromechanical analysis of composites by the generalized cells model. Mech Mater 1992;14:127–39.
[8] Pindera MJ, Bednarcyk BA. An efficient implementation of the generalized method of cells for unidirectional, multi-phased composites with complex microstructures. Composites: Part B 1999;30:87–105.
[9] Graham LL, Baxter SC. Simulation of local material properties based on moving-window GMC. Probabilist Eng Mech 2001;16:295–305.
[10] Camanho PP, Davila CG. Ambur DR. Numerical simulation of delamination growth in composite materials. NASA-TP-211041; 2001.
[11] Tsai SW. Strength theories of filamentary structures. In: Schwartz RT, Schwartz HS, editors. Fundamental aspects of fiber reinforced plastic composites. New York: Wiley Interscience; 1968. p. 3–11.
[12] Tsai SW, Wu EM. A general theory of strength for anisotropic materials. J Compos Mater 1971;5:58–80.
[13] Hashin Z, Rotem A. A fatigue failure criterion for fiber reinforced composite materials. J Compos Mater 1973;7:448–64.
[14] Hashin Z. Failure criteria for unidirectional fiber composites. J Appl Mech 1980;47:329–34.
[15] Sung KH, Kyo KJ, Yuan CH. Micro-mechanics of failure (MMF) for continuous fiber reinforced composites. J Compos Mater 2008;42:1873–95.
[16] Albert MM, Aditi C, Bednarcyk BA, Arnold SM. Micromechanics-based progressive failure analysis of composite laminates using different constituent failure theories. AIAA-2008-1826; 2008.
[17] Bansal Y, Pindera MJ. Finite-volume direct averaging micromechanics of heterogeneous materials with elastic–plastic phases. Int J Plasticity 2006;22:775–825.